Organic Light-Emitting Diodes

International Edition: DOI: 10.1002/anie.201603232
German Edition: DOI: 10.1002/ange.201603232

Aggregation-Induced Delayed Fluorescence Based on Donor/Acceptor-Tethered Janus Carborane Triads: Unique Photophysical Properties of Nondoped OLEDs

*Ryuhei Furue[+], Takuro Nishimoto[+], In Seob Park, Jiyoung Lee, and Takuma Yasuda**

Abstract: *Luminescent materials consisting of boron clusters, such as carboranes, have attracted immense interest in recent years. In this study, luminescent organic–inorganic conjugated systems based on o-carboranes directly bonded to electron-donating and electron-accepting π-conjugated units were elaborated as novel optoelectronic materials. These o-carborane derivatives simultaneously possessed aggregation-induced emission (AIE) and thermally activated delayed fluorescence (TADF) capabilities, and showed strong yellow-to-red emissions with high photoluminescence quantum efficiencies of up to 97% in their aggregated states or in solid neat films. Organic light-emitting diodes utilizing these o-carborane derivatives as a nondoped emission layer exhibited maximum external electroluminescence quantum efficiencies as high as 11%, originating from TADF.*

Organic materials with efficient solid-state emission are essential for various optoelectronic applications, especially for organic light-emitting diodes (OLEDs).[1] However, the efficient luminescence detected for most organic fluorophores in dilute solutions is generally weakened or quenched when the molecules aggregate in their condensed solid states. This effect is because of aggregation-caused emission quenching (so-called concentration quenching) and is attributed to nonradiative deactivation processes, such as excitonic coupling, excimer formation, and intermolecular excitation energy transfer. Therefore, for OLEDs, organic fluorophores are generally used as a dopant (guest emitter) dispersed in an appropriate host matrix, whereas the application of nondoped materials is restricted. Moreover, efficacious doping often requires precise control of the doping concentration in order to suppress serious efficiency roll-off caused by exciton annihilation in the devices at high doping concentrations and high current densities. To simplify the device structures and fabrication processes, it is desirable to construct highly efficient OLEDs with nondoped (neat) emission layers.

In 2001, Tang and co-workers discovered an intriguing photophysical phenomenon termed aggregation-induced emission (AIE), which has been proved to be an effective approach to suppress concentration quenching and hence to attain efficient solid-state luminescence.[2] Thus far, a series of AIE-active fluorophores, including siloles,[2,3] cyanostilbenes,[4] tetraphenylethenes,[5] and *o*-carborane derivatives,[6] has been reported. These molecules are essentially nonluminescent in dilute solutions but become highly emissive upon formation of aggregates. On this basis, some AIE-active fluorophores have been developed as emitters for efficient nondoped OLEDs.[5,7] However, these fluorescent devices still utilize only the singlet (S_1) excitons for electroluminescence (EL); these excitons correspond to about 25% of the total electro-generated excitons, whereas employing the remaining unharvested 75% triplet (T_1) excitons could potentially lead to molecular systems with enhanced EL properties.

o-Carborane (1,2-*closo*-dicarbadodecaborane ($C_2B_{10}H_{12}$)) is known as an electron-deficient icosahedral boron cluster consisting of three-center two-electron bonds, and possesses highly polarizable σ-aromatic character.[8] This unique feature allows the carborene cage to interact electronically with π-conjugated systems attached through the carbon atoms. Chujo and Kokado reported a series of luminescent *o*-carborane derivatives substituted with various electron-donating and electron-withdrawing aromatic groups that were applied to color-tunable AIE-active systems.[6a] Research interest has also focused on the use of *o*-carborane cages as building blocks to explore new optoelectronic functional materials, including organic small molecules,[6a–c,9] polymers,[6d–f,10] and metal complexes.[11] However, the detailed photophysical properties of carborane-based AIE-active molecules and their potential applicability as emitters in OLED devices have not been fully elucidated to date.

In this Communication, we report a novel class of AIE-active organic–inorganic conjugated systems based on *o*-carboranes tethered with donor (D) and acceptor (A) moieties (denoted "Janus" carboranes **1**–**3**; Figure 1). It is found that these triad molecules can harvest both S_1 and T_1 excitons and display thermally activated delayed fluorescence[12] through upconversion from nonradiative T_1 excitons into emissive S_1 excitons in their aggregated states. As a consequence of such unique aggregation-induced delayed fluorescence (AIDF) ability,[13] high external EL quantum

[*] R. Furue,[+] I. S. Park, J. Lee, Prof. Dr. T. Yasuda
INAMORI Frontier Research Center (IFRC), Kyushu University
744 Motooka, Nishi-ku, Fukuoka 819-0395 (Japan)
E-mail: yasuda@ifrc.kyushu-u.ac.jp
Homepage: http://www.inamori-frontier.kyushu-u.ac.jp/optoelectronics/
R. Furue,[+] J. Lee, Prof. Dr. T. Yasuda
Department of Automotive Science, Graduate School of Integrated Frontier Science, Kyushu University
744 Motooka, Nishi-ku, Fukuoka 819-0395 (Japan)
T. Nishimoto,[+] I. S. Park, Prof. Dr. T. Yasuda
Department of Applied Chemistry
Graduate School of Engineering, Kyushu University
744 Motooka, Nishi-ku, Fukuoka 819-0395 (Japan)
[+] These authors are contributed equally to this work.

Supporting information for this article can be found under: http://dx.doi.org/10.1002/anie.201603232.

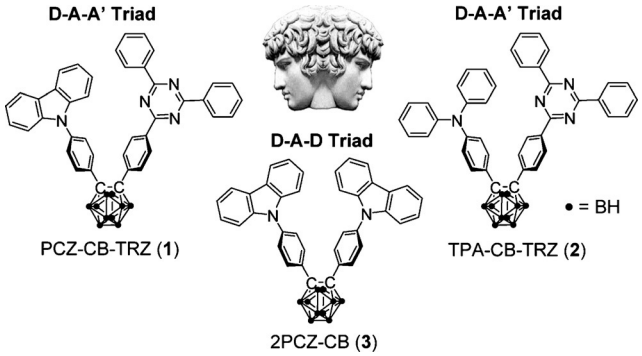

Figure 1. Structural formulae of Janus carboranes **1**–**3** (Janus is a Roman god and is depicted having two faces).

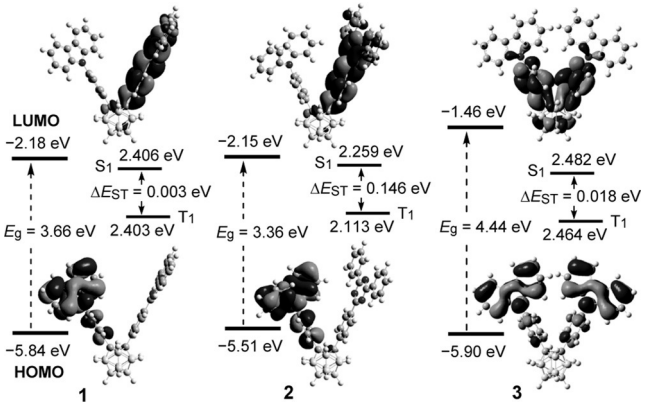

Figure 2. HOMO and LUMO distributions and calculated singlet (S_1) and triplet (T_1) energy levels for **1**–**3** based on TDDFT at the PBE1PBE/6-31G(d) level.

efficiencies (η_{ext}) of over 10% could be achieved in OLEDs by employing **1**–**3** as nondoped (neat) emission layers.

The key design strategy for AIDF molecules is to minimize the spatial overlap between their HOMO and LUMO by localizing these orbitals on different moieties in a single molecule, leading to a small S_1–T_1 energy splitting (ΔE_{ST}) and enabling efficient upconversion from the T_1 to the S_1 state through reverse intersystem crossing (RISC).[12] Based on this requirement, we designed novel D–A–A′ triads **1** and **2** by incorporating a 9-phenylcarbazole or triphenylamine moiety (D) and a 2,4,6-triphenyl-1,3,5-triazine moiety (A′) into a central *o*-carborane core (A) at the C_1 and C_2 positions (Figure 1). To verify the effect of the structural modulation on the photophysical properties, D–A–D triad **3** possessing two 9-phenylcarbazole units was also prepared.[9] Compounds **1**–**3** were synthesized from decaborane ($B_{10}H_{14}$) and the corresponding disubstituted acetylenes in moderate yields (33–49%), and their structures were characterized by NMR spectroscopy, mass spectrometry, and elemental analysis after purification by temperature-gradient vacuum sublimation (see the Supporting Information for details). X-ray crystallographic analysis of **1**[14] revealed that the C_1–C_2 distance in the *o*-carborane cage (1.714 Å) is much longer than that in the nonsubstituted *o*-carborane (1.629 Å).[15] This elongation of the C_1–C_2 bond can be attributed to conjugation with D and A substituents at the cage carbon atoms.

The frontier orbital distributions and excited energy levels were investigated using time-dependent density functional theory (TDDFT) calculations. Figure 2 shows that the HOMOs of **1** and **2** are located on the respective D moieties, whereas the corresponding LUMOs are mainly distributed over the peripheral A′ moieties. Accordingly, **1** and **2** provide evident spatial separation of the HOMO and LUMO distributions, resulting in small calculated ΔE_{ST} values of 0.003 and 0.146 eV, respectively. The replacement of a phenylcarbazole unit with a triphenylamine unit in **2** results in a slight increase of the ΔE_{ST} value, owing to a larger spatial overlap of the frontier orbitals. The HOMO→LUMO electronic transition dominates the lowest-energy S_1 excitation for **1** and **2**, providing evidence for the notable intramolecular charge transfer (ICT) character of these species. Unlike the asymmetric triads **1** and **2** in which the *o*-carborane core serves as a bulky bridging hub offering very weak electronic connectivity between the two peripheral units, the symmetric triad **3** appears to have very different frontier orbital distributions. In the case of **3**, the LUMO is predominantly localized on the central 1,2-diphenylcarborane moiety, which functions as an electron-accepting unit rather than a hub for anchoring the peripheral π-conjugated groups. Thus, the ΔE_{ST} of **3** is calculated to be 0.018 eV, which is also small enough to induce efficient RISC.

Photoluminescence (PL) spectroscopic analyses of the Janus carboranes in THF/water mixtures revealed their AIE characteristics (Figure 3 a,b). We used THF and water as the solvent pair given that the good solvent and the poor solvent should be adequately miscible. In pure THF solution, molecularly dissolved **1** exhibited very weak blue emission bands centered at 346 and 467 nm with a PL quantum yield (Φ_{PL}) of only 3% (Table 1), which can be assigned to fluorescence from the locally excited (LE) states of the phenylcarbazole and triphenyltriazine moieties. With an increase of the water fraction (f_w), the intensity of the LE emission bands became negligible at f_w values larger than 70%. Meanwhile, a bright yellow emission band emerged at longer wavelengths ($\approx$590 nm), originating from the lowest-energy ICT excited state; the intensity of this emission band increased significantly with the formation of aggregates. The Φ_{PL} of **1** increased to over 50% in the THF/water mixture with $f_w = 90\%$, indicative of AIE-active behavior. Similar PL changes were also detected for **2** and **3** in aqueous mixtures (Supporting Information). It is assumed that the AIE originates primarily from restriction of the intramolecular rotations of the peripheral D and A′ moieties. In dilute solutions, the multiple aromatic rings in **1**–**3** can rotate, resulting in dissipation of the excitation energy as thermal energy. However, when the carborane molecules aggregate, the rotation of the peripheral units, which lead to nonradiative decay, are effectively impeded, and thus the molecules become strongly emissive.

We further studied the PL properties of **1**–**3** as vacuum-deposited neat films for practical applications. The neat films of **1**–**3** show broad and structureless PL emissions with peaks (λ_{PL}) at 557, 624, and 571 nm, respectively (Table 1). These PL

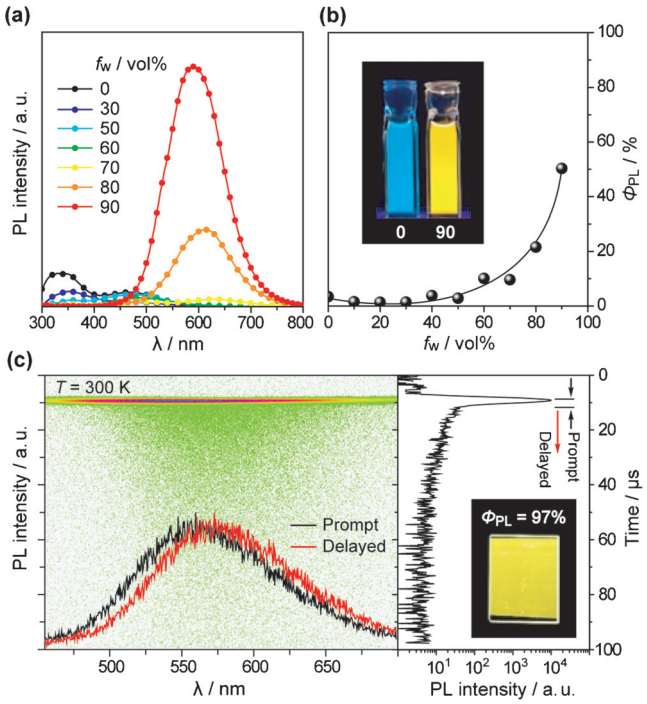

Figure 3. a) PL spectra of **1** in THF/water mixtures with different water fractions (f_w). b) Plots of absolute PL quantum yields (Φ_{PL}) versus f_w of the aqueous mixtures. Inset in (b): fluorescence images of **1** in pure THF ($f_w = 0\%$) and in a THF/water mixture ($f_w = 90\%$) under UV light irradiation. c) Streak image and prompt and delayed emission spectra (left) and transient PL decay profile (right) of a neat film of **1** obtained at 300 K (inset: photograph of yellow PL from the neat film). Green dots in the streak image in (c) represent PL photon counts.

profiles are similar to those of the corresponding aggregated states in THF/water mixtures. Although the Φ_{PL} values of **1–3** in THF solutions were merely 1–3%, those of their neat films increased to 97%, 55%, and 94%, respectively, demonstrating that the AIE-active Janus carboranes indeed function as excellent solid-state emitters. More intriguingly, the transient PL decay of the neat film of **1** clearly revealed two exponential decay components (Figure 3c) consisting of a prompt PL decay with a transient lifetime (τ_p) of 15 ns and a delayed decay with a lifetime (τ_d) of 27 µs. The spectral profile of the delayed PL emission is almost superimposable on the prompt fluorescence profile from the S_1 state (that is, the lowest singlet ICT excited state) but with a much longer transient lifetime. Thus, we conclude that the delayed component is attributed to AIDF. At ambient temperature (300 K), the upper-lying S_1 state is significantly populated by upconversion from the lower-lying T_1 states by means of thermal activation, leading to AIDF. From the overall Φ_{PL} value and the proportions of the integral areas of these two components in the transient PL decay curve, the fractional quantum efficiencies for the prompt (Φ_p) and delayed (Φ_d) components of **1** in the neat film were estimated to be 90% and 7%, respectively. Detailed photophysical data for **1–3** are summarized in Table 1. It is noteworthy that the D–A–D triad **3** also possesses AIDF properties (Supporting Information), despite the lack of the triphenyltriazine acceptor moiety as an additional A′ unit. Considering the strong electron-withdrawing ability of *o*-carborane, the emission from **3** in the neat film may be ascribed to an ICT process that occurs between the π-system of the electron-donating phenylcarbazole moieties and the carborane cage. Thus, *o*-carborane also plays a pivotal role for the generation of AIDF in **3**.

The unique AIDF properties of the Janus carboranes **1–3** with efficient solid-state emission inspired us to evaluate their EL performance in nondoped OLEDs. OLED devices (Figure 4a) were fabricated with the ITO/α-NPD (35 nm)/mCP (10 nm)/EML (20 nm)/PPT (40 nm)/LiF (0.8 nm)/Al (80 nm) configuration (ITO = indium tin oxide; α-NPD = 4,4′-bis-[*N*-(1-naphthyl)-*N*-phenylamino]-1,1′-biphenyl; mCP = 1,3-bis(carbazol-9-yl)benzene; EML = emission layer; PPT = 2,8-bis(diphenylphosphoryl)dibenzo[*b*,*d*]thiophene).[16] In these devices, **1–3** functioned as a nondoped EML, α-NPD and PPT served as a hole-transporting layer and an electron-transporting layer, respectively, and mCP acted as an electron-blocking layer.

Figures 4b and 4c show the current density–voltage–luminance (*J*–*V*–*L*) and η_{ext}–*J* characteristics of the fabricated OLEDs. Nondoped OLEDs incorporating **1** and **3** as an EML emitted bright yellow light with EL maxima (λ_{EL}) at 586 and 590 nm, respectively, which were red-shifted to some degree relative to the PL emission maximum of their neat films. Similarly, red EL emission with $\lambda_{EL} = 631$ nm was solely observed from the device with **2**, suggesting that the holes and electrons were injected with a good balance and that the charge recombination zone is confined inside the nondoped EML. The turn-on voltage of the device employing **1** ($V_{on} = 6.3$ V) was higher than those of the devices with **2** and **3** ($V_{on} = 4.4$ V) because of the larger hole-injection barrier at the mCP/EML interface resulting from the deeper-lying HOMO energy level of **1** (see Table 1). However, the OLED

Table 1: Photophysical properties of Janus carboranes **1–3**.

Compound	λ_{abs} [nm] sol[a]	λ_{PL} [nm] sol[a]/film[b]	Φ_{PL}[c] [%] sol[a]/film[b]	τ_p[d] [ns]	τ_d[d] [µs]	HOMO[e] [eV]	LUMO[f] [eV]	E_g[g] [eV]	ΔE_{ST}[h] [eV]
PCZ-CB-TRZ (**1**)	278, 322[i], 336[i]	346, 467[i] / 557	3 / 97	15	27	−6.40	−3.05	3.35	0.003
TPA-CB-TRZ (**2**)	278, 323[i]	533 / 624	3 / 55	10	–[j]	−6.24	−3.60	2.64	0.146
2PCZ-CB (**3**)	292, 323[i], 337[i]	350 / 571	1 / 94	13	28	−6.33	−2.80	3.53	0.018

[a] Measured in oxygen-free THF solution at RT. [b] Neat film deposited on a quartz substrate. [c] Absolute PL quantum yield evaluated using an integrating sphere under N_2. [d] PL lifetimes of prompt (τ_p) and delayed (τ_d) decay components for neat films measured using a streak camera at 300 K under vacuum. [e] Determined by photoelectron yield spectroscopy in neat films. [f] LUMO = HOMO + E_g. [g] Optical energy gap (E_g) deduced from the absorption onset of a neat film. [h] Calculated by TDDFT at the PBE1PBE/6-31G(d) level. [i] Shoulder or sub peak. [j] Not determined.

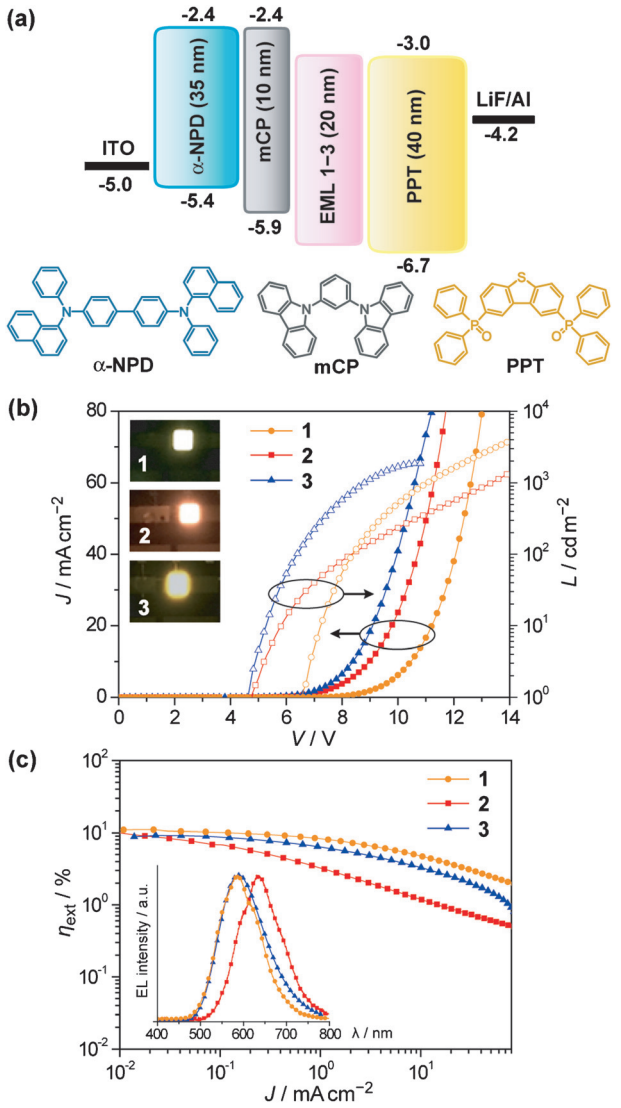

Figure 4. a) Schematic energy level diagram of nondoped OLEDs based on **1**–**3** and the molecular structures of the materials used. b) Current density–voltage–luminance (*J*–*V*–*L*) characteristics (inset: EL emission images) and c) external EL quantum efficiency (η_{ext}) as a function of *J* values for the fabricated OLEDs (inset: EL spectra measured at 10 mA cm^{-2}).

incorporating **1** exhibited the highest η_{ext} value of up to 11.0% and the maximum luminance of 4530 cd m^{-2} among all the evaluated devices (Figure 4b,c), given that the neat film of **1** presents the highest Φ_{PL} value (97%). Although relatively lower maximum η_{ext} values were obtained for the devices with **2** and **3** (η_{ext} = 10.1% and 9.2%, respectively), the EL efficiencies of these devices far exceeded the theoretical limit for conventional fluorescent OLEDs. In general, the maximum theoretical η_{ext} for OLEDs is expressed by Equation (1):

$$\eta_{ext} = \eta_{int} \times \eta_{out} = (\gamma \times \eta_{ST} \times \Phi_{PL}) \times \eta_{out} \quad (1)$$

where η_{int} is the internal EL quantum efficiency, η_{out} is the light out-coupling efficiency (typically $\eta_{out} \approx 0.2$), γ is the charge balance factor (ideally $\gamma = 1$), and η_{ST} is the fraction of radiative excitons ($\eta_{ST} = 0.25$ for fluorescence emitters). If **1**–**3** are assumed to be normal fluorescent emitters, their theoretical η_{ext} values should be restricted to about 4.9%, 2.8%, and 4.7%, respectively, by assuming an η_{ST} value of 25% based on the spin statistical limit. However, the actual η_{ext} values for the OLEDs employing **1**–**3** were noticeably higher than those calculated by using Equation (1). Therefore, these results unambiguously demonstrate that the electro-generated T_1 excitons are utilized effectively for the generation of EL emission through viable RISC processes in Janus carboranes that act as novel AIDF emitters.

In summary, we have developed a series of *o*-carborane-based fluorophores, **1**–**3**, that exhibit high PL quantum efficiencies of up to 97% in solid-state neat films. The unique electronic and geometric features of these *o*-carborane-based π-systems can be harnessed in efficient delayed fluorescence materials that simultaneously exhibit AIE characteristics. A nondoped OLED employing **1** as an emitter demonstrated an external EL quantum efficiency as high as 11.0%, which is considerably higher than those obtained with conventional fluorescent emitters. This design strategy for AIDF materials will offer new prospects for the realization of high-performance nondoped optoelectronic devices.

Acknowledgements

This work was partially supported by the JST ACCEL project and a Grant-in-Aid for Scientific Research (Nos. 15H01049 "3D Active-Site Science", 25708032, and 26620168) from JSPS, the Ogasawara Foundation for the Promotion of Science and Engineering, the Kurata Memorial Hitachi Science and Technology Foundation, the Kumagai Foundation for Science and Technology, the Sumitomo Electric Group CSR Foundation, the Futaba Electronics Memorial Foundation, and the Canon Foundation.

Keywords: carboranes · delayed fluorescence · organic light-emitting diodes · photophysical properties · semiconductors

How to cite: *Angew. Chem. Int. Ed.* **2016**, *55*, 7171–7175
Angew. Chem. **2016**, *128*, 7287–7291

[1] a) *Organic Light-Emitting Devices: Synthesis Properties and Applications* (Eds.: K. Müllen, U. Scherf), Wiley-VCH, Weinheim **2006**; b) A. C. Grimsdale, K. L. Chan, R. E. Martin, P. G. Jokisz, A. B. Holmes, *Chem. Rev.* **2009**, *109*, 897–1091; c) M. Shimizu, T. Hiyama, *Chem. Asian J.* **2010**, *5*, 1516–1531; d) L. Xiao, Z. Chen, B. Qu, J. Luo, S. Kong, Q. Gong, J. Kido, *Adv. Mater.* **2011**, *23*, 926–952.
[2] a) J. Luo, Z. Xie, J. W. Y. Lam, L. Cheng, H. Chen, C. Qiu, H. S. Kwok, X. Zhan, Y. Liu, D. Zhu, B. Z. Tang, *Chem. Commun.* **2001**, 1740–1741; b) B. Z. Tang, X. Zhan, G. Yu, P. P. S. Lee, Y. Liu, D. Zhu, *J. Mater. Chem.* **2001**, *11*, 2974–2978; c) J. Mei, Y. Hong, J. W. Y. Lam, A. Qin, Y. Tang, B. Z. Tang, *Adv. Mater.* **2014**, *26*, 5429–5479.
[3] Z. Zhao, B. He, B. Z. Tang, *Chem. Sci.* **2015**, *6*, 5347–5365.
[4] B.-K. An, J. Gierschner, S. Y. Park, *Acc. Chem. Res.* **2012**, *45*, 544–554.

[5] Z. Zhao, J. W. Y. Lam, B. Z. Tang, *J. Mater. Chem.* **2012**, *22*, 23726 – 23740, and references therein.
[6] a) K. Kokado, Y. Chujo, *J. Org. Chem.* **2011**, *76*, 316 – 319; b) L. Weber, J. Kahlert, R. Brockhinke, L. Böhling, A. Brockhinke, H.-G. Stammler, B. Neumann, R. A. Harder, M. A. Fox, *Chem. Eur. J.* **2012**, *18*, 8347 – 8357; c) S.-Y. Kim, Y.-J. Cho, G. F. Jin, W.-S. Han, H.-J. Son, D. W. Cho, S. O. Kang, *Phys. Chem. Chem. Phys.* **2015**, *17*, 15679 – 15682; d) K. Kokado, Y. Chujo, *Macromolecules* **2009**, *42*, 1418 – 1420; e) K. Kokado, Y. Tokoro, Y. Chujo, *Macromolecules* **2009**, *42*, 9238 – 9242; f) J. J. Peterson, M. Were, Y. C. Simon, E. B. Coughlin, K. R. Carter, *Macromolecules* **2009**, *42*, 8594 – 8598.
[7] For recent examples, see: a) Y. Liu, S. Chen, J. W. Y. Lam, P. Lu, R. T. K. Kwok, F. Mahtab, H. S. Kwok, B. Z. Tang, *Chem. Mater.* **2011**, *23*, 2536 – 2544; b) X. Du, J. Qi, Z. Zhang, D. Ma, Z. Y. Wang, *Chem. Mater.* **2012**, *24*, 2178 – 2185; c) J. Y. Kim, T. Yasuda, Y. S. Yang, C. Adachi, *Adv. Mater.* **2013**, *25*, 2666 – 2671; d) J. Huang, N. Sun, Y. Dong, R. Tang, P. Lu, P. Cai, Q. Li, D. Ma, J. Qin, Z. Li, *Adv. Funct. Mater.* **2013**, *23*, 2329 – 2337; e) L. Chen, Y. Jiang, H. Nie, P. Lu, H. H. Y. Sung, I. D. Williams, H. S. Kwok, F. Huang, A. Qin, Z. Zhao, B. Z. Tang, *Adv. Funct. Mater.* **2014**, *24*, 3621 – 3630; f) J. Huang, Y. Jiang, J. Yang, R. Tang, N. Xie, Q. Li, H. S. Kwok, B. Z. Tang, Z. Li, *J. Mater. Chem. C* **2014**, *2*, 2028 – 2036; g) H. Shi, D. Xin, X. Gu, P. Zhang, H. Peng, S. Chen, G. Lin, Z. Zhao, B. Z. Tang, *J. Mater. Chem. C* **2016**, *4*, 1228 – 1237.
[8] a) R. N. Grimes, *Carboranes*, 2nd ed., Academic Press, New York, **2011**; b) R. E. Williams, *Chem. Rev.* **1992**, *92*, 177 – 207; c) V. I. Bregadze, *Chem. Rev.* **1992**, *92*, 209 – 223.
[9] a) K.-R. Wee, Y.-J. Cho, S. Jeong, S. Kwon, J.-D. Lee, I.-H. Suh, S. O. Kang, *J. Am. Chem. Soc.* **2012**, *134*, 17982 – 17990; b) K.-R. Wee, W.-S. Han, D. W. Cho, S. Kwon, C. Pac, S. O. Kang, *Angew. Chem. Int. Ed.* **2012**, *51*, 2677 – 2680; *Angew. Chem.* **2012**, *124*, 2731 – 2734; c) S. Kwon, K.-R. Wee, Y.-J. Cho, S. O. Kang, *Chem. Eur. J.* **2014**, *20*, 5953 – 5960.
[10] a) J. Marshall, B. C. Schroeder, H. Bronstein, I. Meager, S. Rossbauer, N. Yaacobi-Gross, E. Buchaca-Domingo, T. D. Anthopoulos, N. Stingelin, P. Beavis, M. Heeney, *Macromolecules* **2014**, *47*, 89 – 96; b) J. Marshall, Z. Fei, C. P. Yau, N. Yaacobi-Gross, S. Rossbauer, T. D. Anthopoulos, S. E. Watkins, P. Beavis, M. Heeney, *J. Mater. Chem. C* **2014**, *2*, 232 – 239.
[11] a) C. Shi, H. Sun, X. Tang, W. Lv, H. Yan, Q. Zhao, J. Wang, W. Huang, *Angew. Chem. Int. Ed.* **2013**, *52*, 13434 – 13438; *Angew. Chem.* **2013**, *125*, 13676 – 13680; b) A. M. Prokhorov, T. Hofbeck, R. Czerwieniec, A. F. Suleymanova, D. N. Kozhevnikov, H. Yersin, *J. Am. Chem. Soc.* **2014**, *136*, 9637 – 9642; c) X. Li, H. Yan, Q. Zhao, *Chem. Eur. J.* **2016**, *22*, 1888 – 1898.
[12] a) H. Uoyama, K. Goushi, K. Shizu, H. Nomura, C. Adachi, *Nature* **2012**, *492*, 234 – 238; b) Q. Zhang, B. Li, S. Huang, H. Nomura, H. Tanaka, C. Adachi, *Nat. Photonics* **2014**, *8*, 326 – 332; c) S. Y. Lee, T. Yasuda, Y. S. Yang, Q. Zhang, C. Adachi, *Angew. Chem. Int. Ed.* **2014**, *53*, 6402 – 6406; *Angew. Chem.* **2014**, *126*, 6520 – 6524; d) S. Hirata, Y. Sakai, K. Masui, H. Tanaka, S. Y. Lee, H. Nomura, N. Nakamura, M. Yasumatsu, H. Nakanotani, Q. Zhang, K. Shizu, H. Miyazaki, C. Adachi, *Nat. Mater.* **2015**, *14*, 330 – 336; e) M. Numata, T. Yasuda, C. Adachi, *Chem. Commun.* **2015**, *51*, 9443 – 9446; f) I. S. Park, S. Y. Lee, C. Adachi, T. Yasuda, *Adv. Funct. Mater.* **2016**, *26*, 1813 – 1821.
[13] a) S. Xu, T. Liu, Y. Mu, Y.-F. Wang, Z. Chi, C.-C. Lo, S. Liu, Y. Zhang, A. Lien, J. Xu, *Angew. Chem. Int. Ed.* **2015**, *54*, 874 – 878; *Angew. Chem.* **2015**, *127*, 888 – 892; b) Z. Xie, C. Chen, S. Xu, J. Li, Y. Zhang, S. Liu, J. Xu, Z. Chi, *Angew. Chem. Int. Ed.* **2015**, *54*, 7181 – 7184; *Angew. Chem.* **2015**, *127*, 7287 – 7290; c) I. H. Lee, W. Song, J. Y. Lee, *Org. Electron.* **2016**, *29*, 22 – 26.
[14] CCDC 1471124 (**1**) contain the supplementary crystallographic data for this paper. These data can be obtained free of charge from The Cambridge Crystallographic Data Centre.
[15] M. G. Davidson, T. G. Hibbert, J. A. K. Howard, A. Mackinnon, K. Wade, *Chem. Commun.* **1996**, 2285 – 2286.
[16] X. Cai, A. B. Padmaperuma, L. S. Sapochak, P. A. Vecchi, P. E. Burrows, *Appl. Phys. Lett.* **2001**, *79*, 2082.

Received: April 2, 2016
Published online: May 4, 2016

